JOURNAL OF THE MECHANICAL BEHAVIOR OF BIOMEDICAL MATERIALS 38 (2014) 232–241

Available online at www.sciencedirect.com

ScienceDirect

www.elsevier.com/locate/jmbbm

Research Paper

Micro-composite substrates for the study of cell-matrix mechanical interactions

*Pen-hsiu Grace Chao**, *Shou-Chien Sheng*, *Wei-Ren Chang*

Institute of Biomedical Engineering, School and Medicine and School of Engineering, National Taiwan University, Rm 503 Zhanshulou, 1 Sec. 4 Roosevelt Road, Taipei, Taiwan

ARTICLE INFO

Article history:
Received 9 July 2013
Received in revised form
3 December 2013
Accepted 14 January 2014
Available online 28 January 2014

Keywords:
Durotaxis
Biomaterials
Mechanotransduction
Stem cells
Migration

ABSTRACT

The chemical and physical gradients in the native cell microenvironment induce intracellular polarization and control cell behaviors such as morphology, migration and phenotypic changes. Directed cell migration in response to substrate stiffness gradients, known as durotaxis or mechanotaxis, has drawn attention due to its significance in development, metastasis, and wound healing. We developed a microcomposite substrate (μCS) platform with a microfabricated base and collagen hydrogel top to generate physiological linear stiffness gradients without any variation in chemical or transport properties. This platform is compatible with both 2D and 3D cell culturing and can be assembled with common supplies found in most biology labs. Ligament fibroblasts (LFs) and mesenchymal stem cells (MSCs) both respond to the mechanical gradient with directed migration. Interestingly, LFs exhibit higher mechanosensitivity compared with MSCs. Polarized nonmuscle myosin IIB distribution was also found on the μCS gradient, confirming previous reports. This robust system provides an easily accessible platform to study cell mechanosensing and a more physiological microenvironment for cell studies.

1. Introduction

The in situ cell microenvironment is often nonhomogenous and anisotropic. The chemical and physical gradients in the extracellular milieu induce intracellular polarization and controls cell behaviors such as morphology, migration and phenotypic changes (Engler et al., 2006; Lo et al., 2000). Directed cell migration in response to chemical gradients, termed chemotaxis, has been widely studied in the context of development and metastasis (Cimetta et al., 2010; Wang et al., 1994). Directed cell migration in response to substrate stiffness gradients, known as durotaxis or mechanotaxis, has drawn attention recently (Lo et al., 2000; Raab et al., 2012; Tse and Engler, 2011; Wang et al., 2012). Other than the aforementioned context, durotaxis may also be involved in wound healing. For instance, the fibrin clot and platelet and myofibroblastic contractions at the wound site increase local stiffness, thus promoting cell migration toward the wound (Janmey et al., 2009). In addition to migration, substrate stiffness is known to influence cell morphology, cytoskeleton organization, proliferation and phenotypic expressions (Engler et al., 2006; Janmey et al., 2009; Klein et al., 2009; Yeung et al., 2005).

A number of approaches have been utilized to generate stiffness gradients for the study of durotaxis. Polyacrylamide crosslinking can be controlled via lithographic or concentration

*Corresponding author. Tel.: +886 233669830; fax: +886 233665268.
E-mail address: pgchao@ntu.edu.tw (P.-h.G. Chao).

1751-6161/$ - see front matter © 2014 Elsevier Ltd. All rights reserved.
http://dx.doi.org/10.1016/j.jmbbm.2014.01.008

gradients to generate stiffness changes (Byfield et al., 2009; Tse and Engler, 2011). These technologies often require microfluidic devices or clean room access, which are not widely available to biologists. Moreover, changes in polyacrylamide crosslinking and density may change protein tethering behaviors, thus changing the mechanical feedback mechanisms (Trappmann et al., 2012). Another limitation of the polyacrylamide gel is that it is not compatible with 3D cell encapsulation due to its toxicity. Other polymer systems have been developed to control 3D stiffness (Khetan et al., 2013; Legant et al., 2010). However, to our knowledge, few studies have investigated polymeric systems of 3D stiffness gradients, due to the difficulty in controlling cell-polymeric interactions in 3D (Khetan et al., 2013). Hadjipanayi and coworkers generated a wedge-shaped collagen hydrogel, which was then compressed to a uniform thickness, thus resulting in a scaffold of varying density (Hadjipanayi et al., 2009). While cells are maintained in a 3D state in this system, they are subjected to inhomogeneous compression and increases in collagen and ligand density.

Alternatively, studies have utilized hydrogel thickness to modulate the effective surface stiffness (Leong et al., 2010). Mesenchymal stem cells (MSCs) on the thin collagen gels exhibit similar behaviors as those grown on hard substrates and the cells cultured on thick gels behaved similarly as those grown on soft substrates (Feng et al., 2013; Leong et al., 2010). Taking advantage of this approach, we generated a micro-composite substrate (μCS) with gradients by controlling collagen hydrogel thickness with precise microfabricated topography, without changes in collagen density. This approach is completely cell compatible and provides both 2D and 3D capabilities. Moreover, the homogeneous gel density ensures that, in the 3D configuration, cells of the same distance to the gel surface are in the same nutrient/waste environment as well as mechanical conditions. The resulting stiffness gradient is linear within the field of view using a standard 10× objective. Furthermore, the same concept can be applied to a variety of materials available in most life science labs to generate substrates of different stiffness or stiffness gradients.

This versatile and simple platform was validated using MSCs and ligament fibroblasts (LFs). LFs have been shown to express smooth muscle-actin, exhibit phenotypes of contractile myofibroblasts and migrate at wound sites (Murray et al., 2002; Murray and Spector, 1999; Unterhauser et al., 2004). In addition to linear gradients, we also generated patterns to produce a radial gradient to study more complex mechanical cues that may occur during mesenchymal condensation or scar formation (Ghosh et al., 2009; Mammoto and Ingber, 2010; Tse and Engler, 2011). 3D capability of our system was demonstrated by the durotactic behavior of MSCs and the mechanisms behind durotaxis in 2D and 3D were explored.

2. Materials and methods

2.1. Micro-composite substrate (μCS)

The composite substrate was prepared with collagen gel and PDMS (polydimethylsiloxane, Sylgard 184, Dow Corning, USA) microstructure. The PDMS microstructure was fabricated by soft lithography. Briefly, SU-8 2025 photoresist (MicroChem, USA) was spin-coated on a silicon wafer, exposed to UV light through a mask, and developed to form a master with feature heights of 60 μm. PDMS elastomer was prepared with 10% cross-linking agent in PDMS solution and casted on the master at 70 °C for 2 h. Collagen gel (BD, USA, rat tail type I, 1.5 mg/mL) was neutralized according to the manufacturer's protocol and immobilized on the PDMS microstructure by treating the PDMS surface with air plasma for 10 min (Harrick Plasma, USA) and incubated overnight at 37 °C. Plasma is believed to activate PDMS surfaces by changing its hydrophobicity, thus promoting protein immobilization (Chang et al., 2007). Collagen gel height was controlled with silicon spacers (100 and 400 μm thick) and cover glass. The 'window' in the spacers, in which the collagen gel periphery is defined, is 1 cm × 1 cm in size. In control studies, uniform thickness substrates were made by binding collagen gels of specified thickness to smooth PDMS substrates. Fig. 1A illustrates the design of the composite substrates.

2.2. Mechanical measurements

Effective modulus at the surface of composite substrate was determined by nano-indentation analysis using an atomic force microscope (AFM, AsylumResearch MFP-3D-BIO, USA) equipped with a Molecular Force Probe 3D controller. Soft silicon nitride cantilevers (TR400PB, Olympus, USA) with a pyramidal tip (nominated spring constant of 0.02 N/m) were calibrated by the thermal fluctuation method in PBS. The cantilever descended toward the collagen gel at a velocity of 1.98 μm/s to achieve an indentation depth of 1 μm. Force–distance curves were collected and analyzed according to the Hertz model (Rotsch et al., 1999; Rotsch and Radmacher, 2000). The gel was modeled with a Poisson ratio of 0.5 (Leong et al., 2010). Effective moduli across the substrates (parallel to gradient) were obtained every 100 μm. 20 repeated force curves on 10 locations obtained from three samples were used to calculate the average effective modulus for each type of substrate.

2.3. Cell culture

Ligament fibroblasts (LFs) were harvested from anterior cruciate ligaments (ACLs) of young porcine knees via enzymatic digestion. Ligament sections were diced and incubated in 0.2% collagenase solution (Invitrogen, USA) on a shaker overnight. After digestion, the mixture was passed through a 100 μm cell strainer and the isolated LFs were maintained without passaging. Human bone marrow-derived mesenchymal stem cells (MSCs) were kindly provided by Dr. Shih-Chieh Hung at National Yang-Ming University (Tsai et al., 2010). For all studies, MSCs were used at passages 11–20. Unless otherwise noted, cells were seeded at 7000 cell/cm^2 for LFs and 5000 cell/cm^2 for MSCs.

2.4. Cell displacement monitoring

For migration studies, cells were cultured overnight in the composite substrate and fitted into a modified migration chamber as previously described (Chao et al., 2000; Tandon

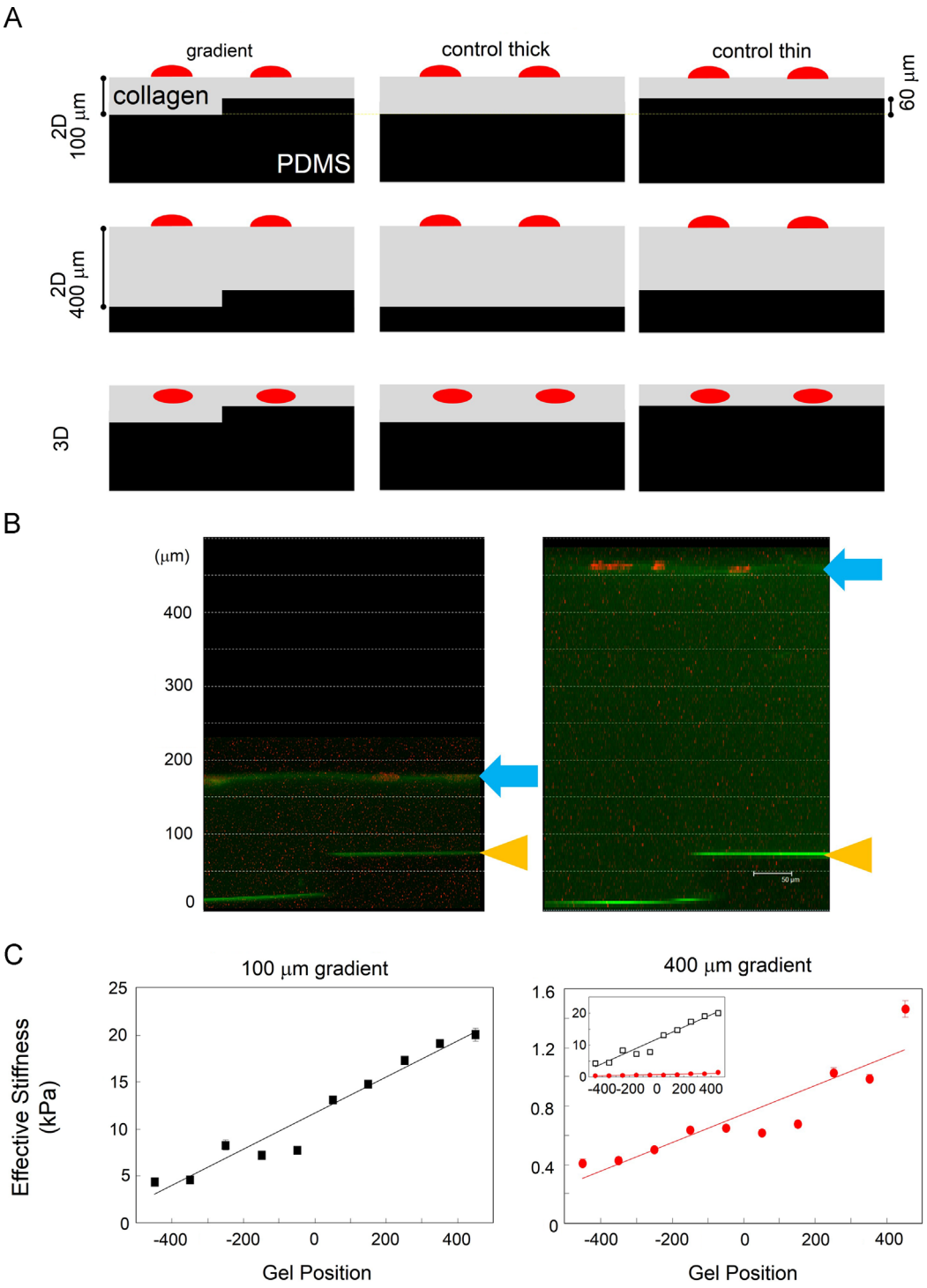

Fig. 1 – Schematic and realization of the μCS. (A) μCS design. (B) Confocal z-stack images of the μCS immediately after cell seeding. Thick blue arrows indicate the cell location and the orange triangles indicate the PDMS–collagen interface in the step region. Green – collagen, red – actin cytoskeleton. (C) AFM assessment of the mechanical properties of the μCS. Red lines indicate linear fits where $R^2=0.95$ and 0.81 for the 100 and 400 μm gradient groups, respectively. Linear trend analysis found $p<0.001$ for both groups. Inserted figure shows the overlay of the two groups. Open black squares represent the 100 μm gradient group and solid red circles represent the 400 μm gradient group. (For interpretation of the references to color in this figure legend, the reader is referred to the web version of this article.)

et al., 2009). The closed chamber was then placed on an inverted microscope (Leica, Germany) and phase-contrast images were taken every 15 min for 1 or 2 h. Fields of view were chosen with the microstructure in the middle, away from the gel edge, and those cells that came into contact with other cells were not analyzed. During the observation period, no significant changes in the focal plane was observed, suggesting low levels of displacement in the z-axis (Feng et al., 2013). Cell location and morphology were measured by manually tracing the cells in Image J to determine the centroid and spreading area of each cell (Fig. 2C) (Abramoff et al., 2004). Cell migration distance and angle (θ) were calculated from the centroid locations of each individual cell with time. Cell directionality was calculated as $\cos\theta$, where θ is the angle between cell displacement axis and the stiffness gradient direction with 0° and indicates that the cell migrated in the direction of the gradient ($\cos\theta=1$).

For the cell enrichment studies, cell-seeded 2D μCS systems were maintained in 6-well plates in a cell culture incubator for 3 days. Cell location was monitored daily by imaging the post and surrounding regions. Cell density was calculated as the cell count normalized by the imaged culture area.

2.5. Cytoskeleton visualization

Fluorescent staining was used to visualize the actomyosin cytoskeleton. Cells were fixed with 3.7% formaldehyde and incubated with Alexa 488-conjugated phalloidin (Invitrogen) to label f-actin. To visualize myosinIIB, the cells were fixed, permeabilized and treated with primary antibodies (Cell Signaling) at 4 °C overnight, followed by secondary antibody labeling (Alexa 568-conjugated, Invitrogen). Florescence signals were imaged with a confocal laser scanning microscope (Leica TCS SP5) with a 20× water-immersion objective.

2.6. Image processing

MyosinIIB distribution was quantified with a custom Matlab program. Images of individual cells were selected and segmented based on the outline of actin cytoskeleton morphology (Chao et al., 2006), which was then divided into four quadrants (Fig. 6B). Average myosinIIB intensity was calculated for each of the four quadrants and normalized to the overall cell intensity. Asymmetry index (AI) was defined as the difference of the average intensity between the quadrant facing the gradient subtracted with the quadrant away from the gradient (Fig. 6). A positive AI value would indicate frontal polarization of myosinIIB (toward the stiffer region, or the right side of the image); where as a negative value would indicate rear polarization.

2.7. Pharmacological studies

Pharmacological agents were used to examine the involvement of various signaling molecules. Blebbistatin (Caymen Chemicals, USA) was used to inhibit myosin II activity. After cells were seeded for a day, 50 μM blebbistatin was added to the cell culture medium for 12 h (Ulrich et al., 2009). In separate studies, rhoA inhibitor exoenzyme C3 transferase (2 μg/ml, Cytoskeleton, USA) was applied in serum-free medium (Provenzano et al., 2008). After treatment, samples were rinsed and supplied with fresh culture medium (with serum) before the migration studies.

2.8. Statistical analysis

Analyses of variance (ANOVA) with post-hoc tests (LSD) were used to investigate multiple comparisons. Significance level (α) was set at 0.05. Statistical analysis was performed using SPSS16 (IBM, USA). Data were reported as mean ± standard errors of the mean.

3. Results

We generated μCS by combining collagen hydrogel with an underlying PDMS substrate with a step topography. As shown in Fig. 1B, by changing the spacer size, we could generate gels of different thicknesses, thus controlling cell distance from the underlying PDMS. This also corresponded with effective material properties. AFM analysis found a significant linear change of mechanical properties across the gel surface within 500 μm of the step topography, approximately the field of view of a regular 10× objective (Fig. 1C). By modifying the total gel thickness with spacers, we generated two μCS at 100 and 400 μm, resulting in stiffness gradients of 17.4 and 1.2 kPa/mm, respectively.

When cells are seeded on this composite substrate, no significant changes can be detected in cell size in response to hydrogel thickness, while MSCs were significantly larger than LFs (Fig. 2A). However, when observed for 2 h, a significant trend of cell migration toward the thinner/stiffer region of the composite substrate can be found in LFs (Fig. 2B). In MSCs, directed migration was only observed in the 100 μm total thickness gradient group, but not in the 400 μm group. Migration in any of the uniform thickness groups were in random directions, resulting in an average $\cos\theta$ value of 0. In both LF and MSCs, cells on the 100 μm gradient demonstrated better migration directionality. When comparing migration speed, LFs on the gradient μCS migrated faster than the cells on the uniform thickness control groups. No such trends could be found with MSCs.

To explore the probability of utilizing this system to simulate mesenchymal condensation (Ghosh et al., 2009) and promote cell enrichment, we designed an alternative μCS in post configuration, where a thin hydrogel region was surrounded by thick gels (Fig. 3A). While there was an initial response of cell enrichment in the central thinner/stiffer region, this effect dissipated after 2 days (Fig. 3B). Note that only minor increases in cell density were observed for the uniform thickness groups. The initial enrichment was also observed in cells treated with mitomycin (data not shown), thus negating a role of proliferation. We investigated this phenomenon by changing the cell seeding density on the μCS with step microstructures. At high cell density, cell directionality as well as migration speed were significantly reduced (Fig. 4A). Further examination found that high seeding density lead to close proximity and cell–cell interactions similar to a tug-of-war (Fig. 4B) and reduced the durotaxis phenomenon on the μCS in post configuration.

When the MSCs were encapsulated in the collagen gel, generating a 3D environment, the cells exhibited similar

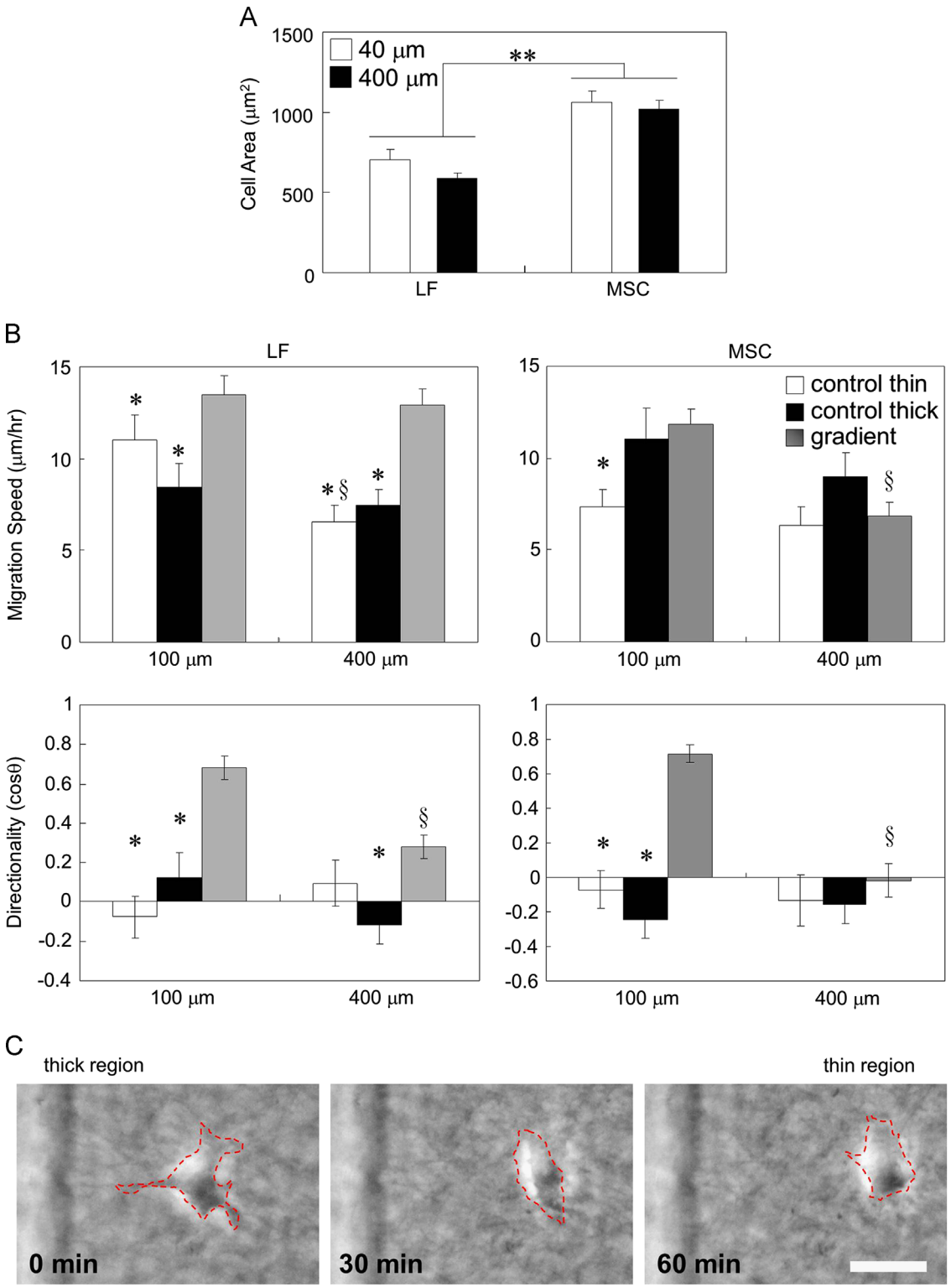

Fig. 2 – (A) Cell size measured on uniform thickness substrates after 24 hours of culture. 40 μm (control thin of the 100 μm-thick gel) and 400 μm (control thick of the 400 μm-thick gel) represent the thinnest and thickest gel thickness used in the current study. ($n=36–46$; ** represents $p<0.001$ when the two indicated groups are compared. No significant differences were found within the indicated groups.) (B) Cell migration response on the μCS. Porcine LF and human MSCs were seeded on the μCS for one day and cell translocation were observed for two hours. ($n=28–80$ for LF and 23–77 for MSCs. * indicates $p<0.05$ compared with the respective gradient group and § indicates $p<0.05$ compared with the respective 100 μm total thickness group) (C) MSC migration on the 100 μm gradient μCS. Scale bar equals 50 μm. (see Supplementary Video 1).

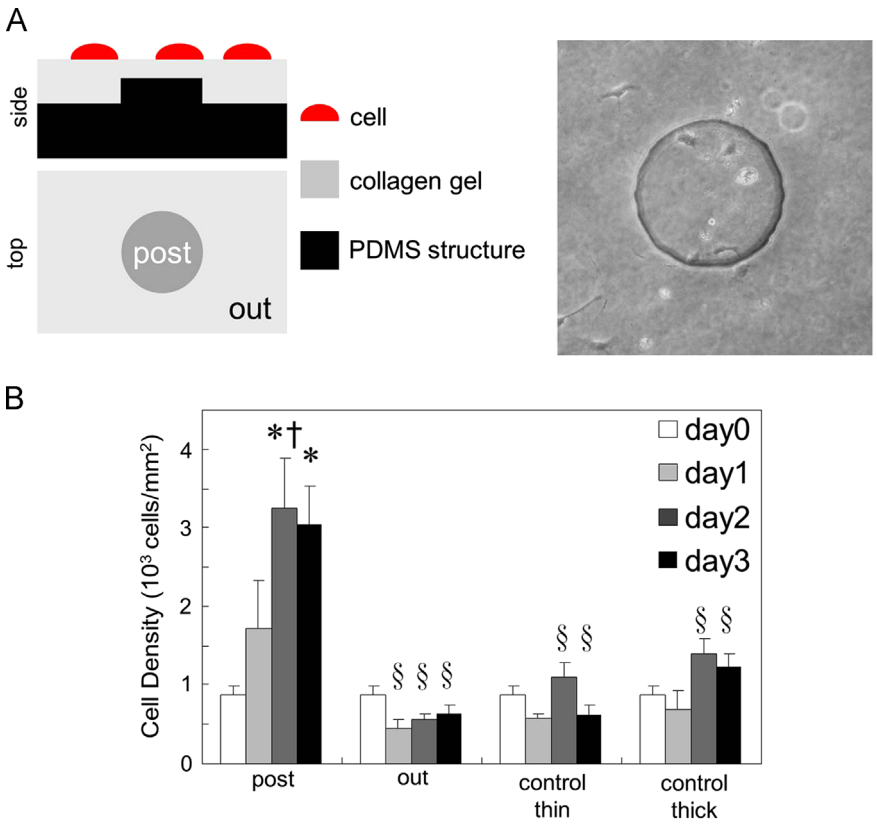

Fig. 3 – (A) The μCS in post configuration. Post diameter is 300 μm. (B) MSC density changes during the three-day culture period on the μCS. (* represents $p<0.0001$ compared with the day 0 group, † indicates $p<0.01$ compared with the previous time point, § indicates $p<0.05$ compared with the post group, $n=4$–20 fields of view).

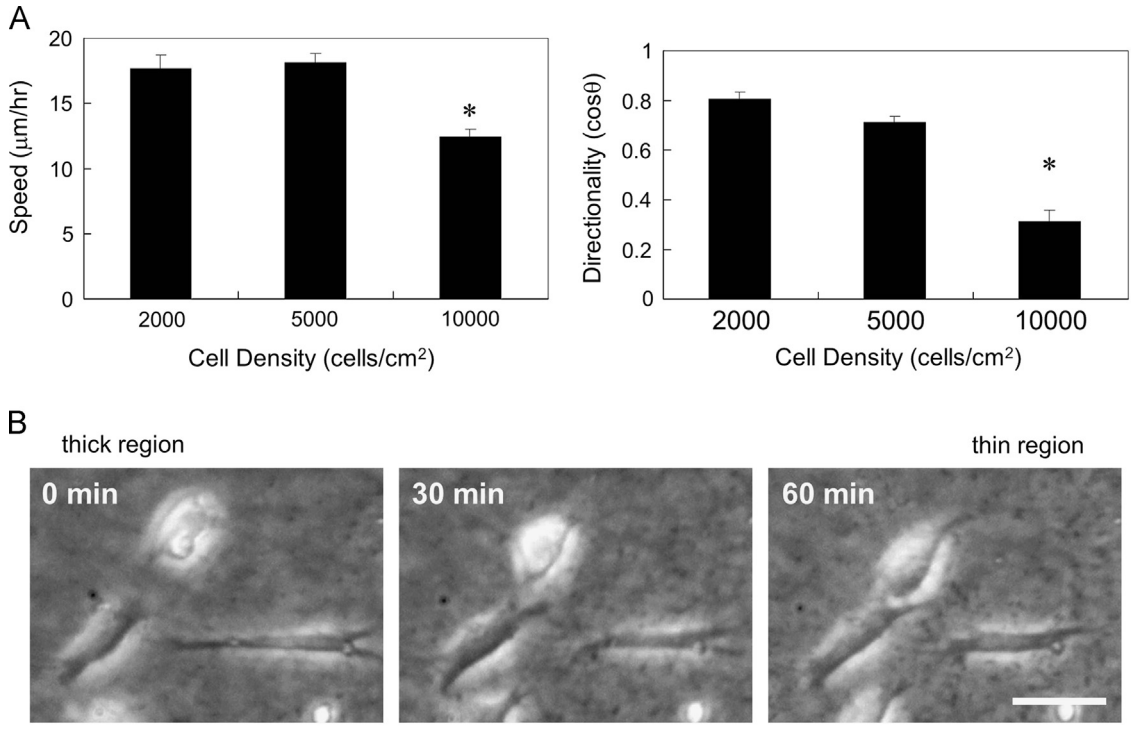

Fig. 4 – (A) Effect of MSC density on μCS directed migration (* represents $p<0.001$ compared with all other groups, $n=120$–232 cells) (B) MSC interactions on the 100 μm gradient substrate (see Supplementary Video 2). Scale bar equals 50 μm.

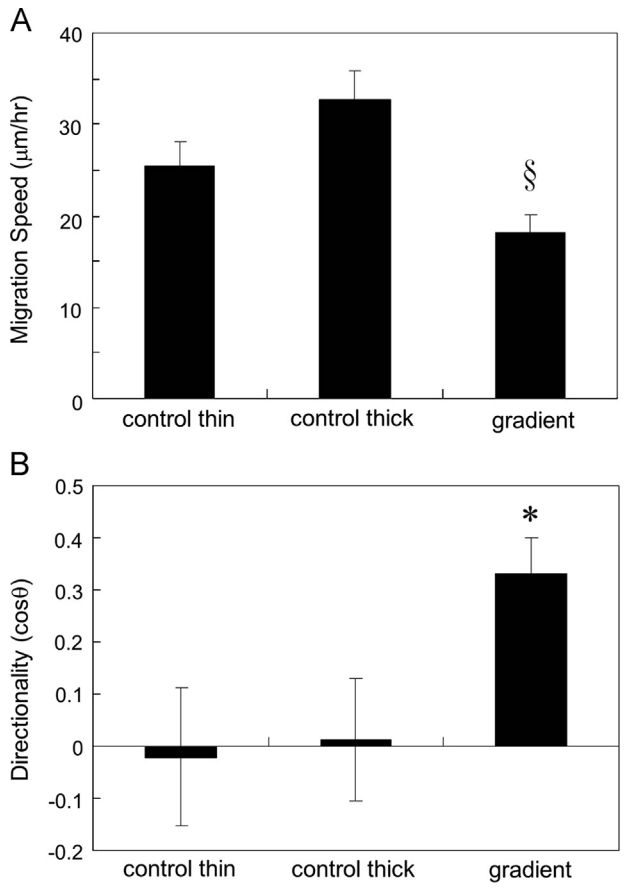

Fig. 5 – MSC migration in the 100 μm-thick 3D μCS. (* represents $p<0.05$ compared with other groups, § indicates $p<0.001$ compared with the thick group, $n=31–39$ cells).

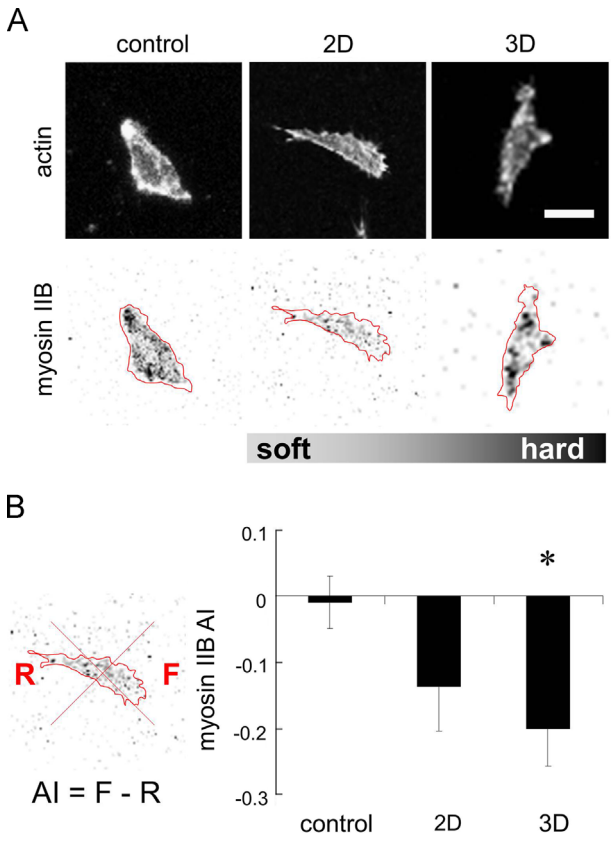

Fig. 6 – Myosin IIB polarization in response to the μCS gradient (A) Actin organization and myosin IIB distribution in the control (flat) substrate as well as on gradient μCS (scale bar equals 20 μm). (B) Quantification of myosin IIB distribution. Asymmetry index (AI) was calculated as the difference of intensity between the region facing the gradient (F) and away from the gradient (R). (* represents $p=0.02$ compared with the control substrate, $n=13–17$).

directionality toward the thinner/stiffer region of the composite substrate, albeit to a lesser degree compared with the 2D system (Fig. 5). Interestingly, migration speed in the uniform thickness groups were about twice as fast as the 2D groups, while the gradient groups migrated at similar speeds.

We next investigated the mechanosensing mechanisms behind the directional migration in the current system. Similar to previous reports on polyacrylamide gradients, nonmuscle myosinIIB demonstrated polarization against the direction of stiffness in both 2D and 3D (Fig. 6) (Raab et al., 2012). Inhibition of myosin II with blebbistatin abolished directional migration on the gradient substrate, with no significant effects on cell migration speed (Fig. 7). Additionally, involvement of the small GTPase rhoA, an upstream regulator of myosin was tested. RhoA inhibition with the C3 exoenzyme revealed a partial inhibition of migration speed and directionality.

4. Discussion

We report a simple yet robust system for generating stiffness gradients in hydrogels that can be used for 2D and 3D culturing. This platform is designed based on controlling the underlying support structure while maintaining a uniform top layer to present an otherwise homogeneous cellular environment. There are recent studies using similar approaches that require complex microfabrication processes (Cortese et al., 2009; Kuo et al., 2012). While we used microfabrication to produce the step features, common lab supplies can be adapted to control topography, such as layering of coverglass, transparency plastics, silicon spacers, or 3D printing. Additionally, extracellular matrix binding to the PDMS can be achieved through chemical treatments instead of plasma, such as via sulpho-SANPAH (Evans et al., 2009; Trappmann et al., 2012). The resulting stiffness gradient can be manipulated to span the physiological and pathological ranges (approximately 1–20 kPa/mm (Tse and Engler, 2011)) by controlling the overall hydrogel thickness and feature height (60 μm in the current study). The absolute stiffness values of the gel can also be regulated to simulate different tissue properties (1∼>100 kPa (Engler et al., 2006)) by defining the absolute thickness of the gel. Other hydrogel parameters can also be adapted easily in the system, such as changing the collagen concentration or using Matrigel or fibrin gels for a wide variety of applications.

Both LF and MSCs exhibited durotaxis on the μCS, although LFs appeared to be more sensitive, responding to the 1.2 kPa/mm gradient at 400 μm thickness (Fig. 2B). The cells may also be responding differently to the different absolute stiffness values

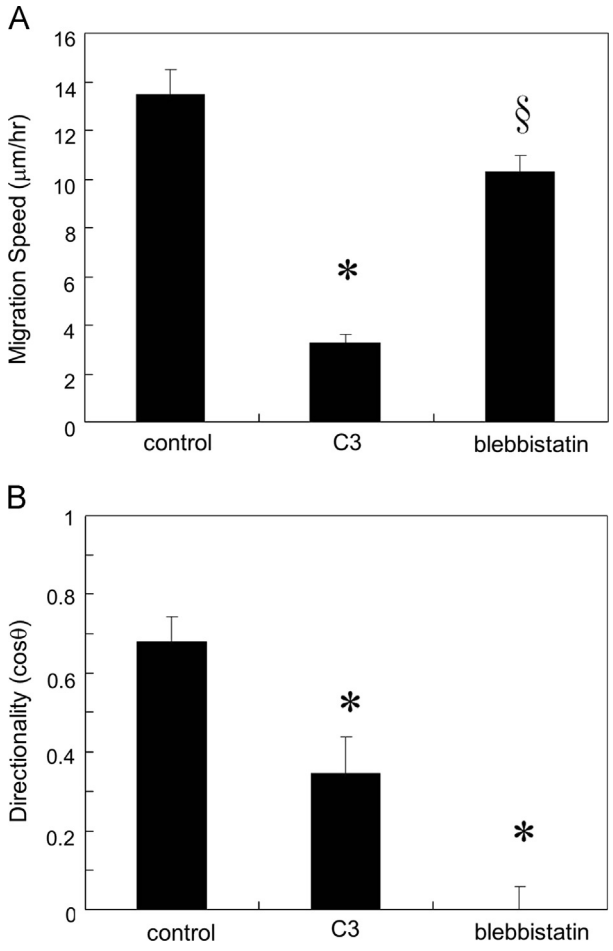

Fig. 7 – Inhibition of RhoA and myosin II modulates directed MSC migration on the μCS. (* represents $p<0.01$ compared with control, § indicates $p<0.05$ compared with the C3 group, $n=58–160$ cells).

in these gradients (0.4–1.2 kPa and 5–20 kPa for the 400 and 100 μm thick gels, respectively). Isenberg and coworkers demonstrated that while cell morphology may be dependent on the absolute stiffness values, durotaxis is dependent on gradient strength (Isenberg et al., 2009). No difference in cell size for either cell type was found between the softest and hardest substrates in the current study (0.4 and 20 kPa, respectively), yet the cells are responding with durotaxis to the mechanical gradient. We recently reported that fibroblasts on collagen gels of different thickness respond differently to substrate anisotropy, while maintaining similar sizes (Feng et al., 2013). Although many studies investigate the effects of substrate mechanical properties by measuring cell size (Lin et al., 2010; Sen et al., 2009), our results suggest that additional parameters can generate a more complete understanding of cellular mechanosensing (Zemel et al., 2010). For instance, neither MSC nor LF exhibited changes in cell size but both demonstrated durotactic behaviors. Modifications in cytoskeleton organization during stem cell differentiation are known to result in different cell stiffnesses (Morita et al., 2013). The disparity between MSC and LF behaviors may therefore be attributed to the different cytoskeleton organizations, leading to distinct mechanosensing and migration mechanisms. The versatility of our novel platform will allow future studies to further investigate the mechanosensing interactions between absolute stiffness and gradient strengths and the cellular mechanisms behind the different phenotypic behaviors.

Cells sense the mechanical environment through attachment sites and cytoskeletal contraction, although the mechanisms are not thoroughly understood (Jiang et al., 2006; Style et al., 2013; Walcott and Sun, 2010). Cell contractility generated from the actomyosin cytoskeleton is one of the key components in the mechanical sensory system (Georges and Janmey, 2005; MacKay et al., 2012). In mechanical gradients, the force balance results in more stable focal adhesions and cytoskeleton bundles on the stiffer side of the gradient and promotes migration in this direction (Bischofs and Schwarz, 2003; Walcott and Sun, 2010). Nonmuscle myosin II isoform phosphorylation and polarization are reported to be involved in this force balance (Lo et al., 2004; Raab et al., 2012). In our μCS system, a similar polarization of myosinIIB against the stiffness/thickness gradient was found in both 2D and 3D (Fig. 6). Moreover, inhibition of myosin or its upstream regulator RhoA suppressed the durotaxis behavior in our system (Fig. 7), confirming previous reports.

Using a comparable stiffness gradient, Tse and coworkers are able to achieve MSC enrichment on photocrosslinked PDMS substrate for seven days. Cell density indeed increased for the first 2 days in our system, suggesting that the mechanical/topographical gradient guided cell migration initially. Cell proliferation is unlikely to result in this increase since the changes in cell density on the control substrates are minor comparatively (Fig. 3B) and mitomycin treatment revealed similar results (data not shown). However, cell migration toward the central thinner/stiffer area ceased beyond day three. A possible mechanism is the nonlinear properties of the collagen gel, where the fibrous network exhibit strain-stiffening behaviors and transmit stresses several cell-lengths away (Ma et al., 2013; Storm et al., 2005; Winer et al., 2009). In contrast to the polymeric gels used in the other study, this heightened nonlinearity allows cells to be influenced by relatively distant objects (Sen et al., 2009). This behavior is evident in our system as demonstrated by the durotaxis response of the smaller LF (length <100 μm) on the 400 μm thick μCS (Fig. 2). The cessation of cell enrichment with time therefore suggests that the increase in density, and decrease in cell–cell distance, result in complex interactions between cells and the mechanical gradient and halt cell durotaxis in our system (Fig. 4).

A number of significant differences have been highlighted between 2D and 3D cell behaviors (Benya and Shaffer, 1982; Cukierman et al., 2001; Doyle et al., 2009). Our system provides a useful platform to study 3D cell behaviors, since the uniform gel density ensures that cells on the same focal plane are exposed to the same nutrient transport and mechanical environment. Furthermore, cell position in the 3D configuration can be more precisely controlled. We previously reported that by taking advantage of the self-assembly behavior of collagen, layered constructs can be generated with specific cell depth in 3D (Feng et al., 2013). Raab and coworkers investigated 3D durotaxis using a gel overlay system (Raab et al., 2012). In agreement with their findings, no differences were found in the myosin-mediated durotaxis between 2D and 3D in our μCS. The migration speeds measured in our system are in the same

order of magnitude as reported in the literature, although somewhat different measures were taken (Raab et al., 2012; Vincent et al., 2013). While different cytoskeletal structures may exist in 2D and 3D systems, the contractile behaviors are similar and can result in similar signaling and force balances (Kraning-Rush et al., 2011). Future studies can combine the current system with traction force microscopy to further delineate the cellular mechanisms behind the contractile and force-sensing behaviors (Wang and Lin, 2007). The ability to provide consistent platforms to study cell behaviors in 2D, 3D, or even combined co-cultures (3D cancer cells with a 2D layer of epithelium, for instance) allows well-controlled investigations into the effects of stiffness gradients on wound healing, metastasis, and development.

5. Conclusions

We developed a μCS platform that allows easy access to mechanical gradient studies. Simple geometry controls such as the single step or post configurations permit a wide array of gradient patterns. Using this system, we are able to generate linear and radial gradients to investigate durotaxis as well as cell enrichment behaviors. Furthermore, the platform can be easily applied in 3D studies with the same chemical and transport parameters, a significant improvement over previous systems. Cells responded to the gradients with directed migration using the same underlying actomyosin mechanism as previous reports. Future studies will investigate the possible interactions between thickness and stiffness gradients, the effects of the nonlinear collagen gel behaviors and coculture systems.

Acknowledgment

The authors would like to acknowledge Dr. Feng-Huei Lin for assistance in AFM and Ms. Wan-ting Yu for technical assistance. We would also like to thank the staff at TC5 Bio-Image Tools, Technology Commons, College of Life Science, National Taiwan University, for assistance with confocal laser scanning microscopy. This work was supported by the Taiwanese National Science Foundation (NSC 101–2221-E-002–045-MY2) and National Health Research Institute (NHRI- EX102-10019EC).

Appendix A. Supplementary materials

Supplementary data associated with this article can be found in the online version at http://dx.doi.org/10.1016/j.jmbbm.2014.01.008.

REFERENCES

Abramoff, M.D., Magelhaes, P.J., Ram, S.J., 2004. Image processing with ImageJ. Biophotonics Int. 11, 36–42.

Benya, P.D., Shaffer, J.D., 1982. Dedifferentiated chondrocytes reexpress the differentiated collagen phenotype when cultured in agarose gels. Cell 30, 215–224.

Bischofs, I.B., Schwarz, U.S., 2003. Cell organization in soft media due to active mechanosensing. Proc. Natl. Acad. Sci. 100, 9274–9279.

Byfield, F.J., Wen, Q., Levental, I., Nordstrom, K., Arratia, P.E., Miller, R.T., Janmey, P.A., 2009. Absence of filamin A prevents cells from responding to stiffness gradients on gels coated with collagen but not fibronectin. Biophys. J. 96, 5095–5102.

Chang, T.Y., Yadav, V.G., De Leo, S., Mohedas, A., Rajalingam, B., Chen, C.-L., Selvarasah, S., Dokmeci, M.R., Khademhosseini, A., 2007. Cell and protein compatibility of parylene-C surfaces. Langmuir 23, 11718–11725.

Chao, P.-H.G., Roy, R., Mauck, R.L., Liu, W., Valhmu, W.B., Hung, C. T., 2000. Chondrocyte translocation response to direct current electric fields. J. Biomech. Eng. 122, 261–267.

Chao, P.-H.G., West, A.C., Hung, C.T., 2006. Chondrocyte intracellular calcium, cytoskeletal organization and gene expression responses to dynamic osmotic loading. Am. J. Physiol. — Cell Physiol. 291, C718–725.

Cimetta, E., Cannizzaro, C., James, R., Biechele, T., Moon, R.T., Elvassore, N., Vunjak-Novakovic, G., 2010. Microfluidic device generating stable concentration gradients for long term cell culture: application to Wnt3a regulation of [small beta]-catenin signaling. Lab Chip 10, 3277–3283.

Cortese, B., Gigli, G., Riehle, M., 2009. Mechanical gradient cues for guided cell motility and control of cell behavior on uniform substrates. Adv. Funct. Mater. 19, 2961–2968.

Cukierman, E., Pankov, R., Stevens, D.R., Yamada, K.M., 2001. Taking cell-matrix adhesions to the third dimension. Science 294, 1708–1712.

Doyle, A.D., Wang, F.W., Matsumoto, K., Yamada, K.M., 2009. One-dimensional topography underlies three-dimensional fibrillar cell migration. J. Cell Biol. 184, 481–490.

Engler, A.J., Sen, S., Sweeney, H.L., Discher, D.E., 2006. Matrix elasticity directs stem cell lineage specification. Cell 126, 677–689.

Evans, N.D., Minelli, C., Gentleman, E., LaPointe, V., Patankar, S.N., Kallivretaki, M., Chen, X., Roberts, C.J., Stevens, M.M., 2009. Substrate stiffness affects early differentiation events in embryonic stem cells. Eur. Cells Mater. 18, 1–14.

Feng, C.-h., Cheng, Y.-c., Chao, P.-h.G., 2013. The influence and interactions of substrate thickness, organization and dimensionality on cell morphology and migration. Acta Biomater. 9, 5502–5510.

Georges, P.C., Janmey, P.A., 2005. Cell type-specific response to growth on soft materials. J. Appl. Physiol. 98, 1547–1553.

Ghosh, S., Laha, M., Mondal, S., Sengupta, S., Kaplan, D.L., 2009. In vitro model of mesenchymal condensation during chondrogenic development. Biomaterials 30, 6530–6540.

Hadjipanayi, E., Mudera, V., Brown, R.A., 2009. Guiding cell migration in 3D: a collagen matrix with graded directional stiffness. Cell Motil. Cytoskelet. 66, 121–128.

Isenberg, B.C., DiMilla, P.A., Walker, M., Kim, S., Wong, J.Y., 2009. Vascular smooth muscle cell durotaxis depends on substrate stiffness gradient strength. Biophys. J. 97, 1313–1322.

Janmey, P.A., Winer, J.P., Murray, M.E., Wen, Q., 2009. The hard life of soft cells. Cell Motil. Cytoskelet. 66, 597–605.

Jiang, G., Huang, A.H., Cai, Y., Tanase, M., Sheetz, M.P., 2006. Rigidity sensing at the leading edge through avb3 integrins and RPTPa. Biophys. J. 90, 1804–1809.

Khetan, S., Guvendiren, M., Legant, W.R., Cohen, D.M., Chen, C.S., Burdick, J.A., 2013. Degradation-mediated cellular traction directs stem cell fate in covalently crosslinked three-dimensional hydrogels. Nat. Mater. 12, 458–465.

Klein, E.A., Yin, L., Kothapalli, D., Castagnino, P., Byfield, F.J., Xu, T., Levental, I., Hawthorne, E., Janmey, P.A., Assoian, R.K., 2009. Cell-cycle control by physiological matrix elasticity and in vivo tissue stiffening. Curr. Biol. 19, 1511–1518.

Kraning-Rush, C., M., Carey, S.P., Califano, J.P., Smith, B.N., Reinhart-King, C.A., 2011. The role of the cytoskeleton in cellular force generation in 2D and 3D environments. Phys. Biol. 8, 015009.

Kuo, C.-H.R., Xian, J., Brenton, J.D., Franze, K., Sivaniah, E., 2012. Complex stiffness gradient substrates for studying mechanotactic cell migration. Adv. Mater. 24, 6059–6064.

Legant, W.R., Miller, J.S., Blakely, B.L., Cohen, D.M., Genin, G.M., Chen, C.S., 2010. Measurement of mechanical tractions exerted by cells in three-dimensional matrices. Nat. Methods 7, 969–971.

Leong, W.S., Tay, C.Y., Yu, H., Li, A., Wu, S.C., Duc, D.-H., Lim, C.T., Tan, L.P., 2010. Thickness sensing of hMSCs on collagen gel directs stem cell fate. Biochem. Biophys. Res. Commun. 401, 287–292.

Lin, Y.-C., Tambe, D.T., Park, C.Y., Wasserman, M.R., Trepat, X., Krishnan, R., Lenormand, G., Fredberg, J.J., Butler, J.P., 2010. Mechanosensing of substrate thickness. Phys. Rev. E 82, 041918.

Lo, C.-M., Buxton, D.B., Chua, G.C.H., Dembo, M., Adelstein, R.S., Wang, Y.-L., 2004. Nonmuscle myosin IIB Is involved in the guidance of fibroblast migration. Mol. Biol. Cell 15, 982–989.

Lo, C.-M., Wang, H.-B., Dembo, M., Wang, Y.-l., 2000. Cell movement is guided by the rigidity of the substrate. Biophys. J. 79, 144–152.

Ma, X., Schickel, M.E., Stevenson, Mark D., Sarang-Sieminski, Alisha L., Gooch, Keith J., Ghadiali, Samir N., Hart, Richard T., 2013. Fibers in the extracellular matrix enable long-range stress transmission between cells. Biophys. J. 104, 1410–1418.

MacKay, Joanna L., Keung, Albert J., Kumar, S., 2012. A genetic strategy for the dynamic and graded control of cell mechanics, motility, and matrix remodeling. Biophys. J. 102, 434–442.

Mammoto, T., Ingber, D.E., 2010. Mechanical control of tissue and organ development. Development 137, 1407–1420.

Morita, Y., Mukai, T., Ju, Y., Watanabe, S., 2013. Evaluation of stem cell-to-tenocyte differentiation by atomic force microscopy to measure cellular elastic moduli. Cell Biochem. Biophys. 66, 73–80.

Murray, M.M., Bennett, R., Zhang, X., Spector, M., 2002. Cell outgrowth from the human ACL in vitro: regional variation and response to TGF-beta1. J. Orthop. Res. 20, 875–880.

Murray, M.M., Spector, M., 1999. Fibroblast distribution in the anteromedial bundle of the human anterior cruciate ligament: the presence of alpha-smooth muscle actin-positive cells. J. Orthop. Res. 17, 18–27.

Provenzano, P.P., Inman, D.R., Eliceiri, K.W., Trier, S.M., Keely, P.J., 2008. Contact guidance mediated three-dimensional cell migration is regulated by Rho/ROCK-dependent matrix reorganization. Biophys. J. 95, 5374–5384.

Raab, M., Swift, J., Dingal, P.C.D.P., Shah, P., Shin, J.-W., Discher, D.E., 2012. Crawling from soft to stiff matrix polarizes the cytoskeleton and phosphoregulates myosin-II heavy chain. J. Cell Biol. 199, 669–683.

Rotsch, C., Jacobson, K., Radmacher, M., 1999. Dimensional and mechanical dynamics of active and stable edges in motile fibroblasts investigated by using atomic force microscopy. Proc. Natl. Acad. Sci. USA 96, 921–926.

Rotsch, C., Radmacher, M., 2000. Drug-induced changes of cytoskeletal structure and mechanics in fibroblasts: an atomic force microscopy study. Biophys. J. 78, 520–535.

Sen, S., Engler, A., Discher, D., 2009. Matrix strains induced by cells: computing how far cells can feel. Cell Mol. Bioeng. 2, 39–48.

Storm, C., Pastore, J.J., MacKintosh, F.C., Lubensky, T.C., Janmey, P.A., 2005. Nonlinear elasticity in biological gels. Nature 435, 191–194.

Style, R.W., Che, Y., Park, S.J., Weon, B.M., Je, J.H., Hyland, C., German, G.K., Power, M.P., Wilen, L.A., Wettlaufer, J.S., Dufresne, E.R., 2013. Patterning droplets with durotaxis. Proc. Natl. Acad. Sci. 110, 12541–12544.

Tandon, N., Cannizzaro, C., Chao, P.-H.G., Maidhof, R., Marsano, A., Au, H.T.H., Radisic, M., Vunjak-Novakovic, G., 2009. Electrical stimulation systems for cardiac tissue engineering. Nat. Protocols 4, 155–173.

Trappmann, B., Gautrot, J.E., Connelly, J.T., Strange, D.G.T., Li, Y., Oyen, M.L., Cohen Stuart, M.A., Boehm, H., Li, B., Vogel, V., Spatz, J.P., Watt, F.M., Huck, W.T.S., 2012. Extracellular-matrix tethering regulates stem-cell fate. Nat. Mater. 11, 642–649.

Tsai, C.-C., Chen, C.-L., Liu, H.-C., Lee, Y.-T., Wang, H.-W., Hou, L.-T., Hung, S.-C., 2010. Overexpression of hTERT increases stem-like properties and decreases spontaneous differentiation in human mesenchymal stem cell lines. J. Biomed. Sci. 17, 64.

Tse, J.R., Engler, A.J., 2011. Stiffness gradients mimicking in vivo tissue variation regulate mesenchymal stem cell fate. PLoS ONE 6, e15978.

Ulrich, T.A., de Juan Pardo, E.M., Kumar, S., 2009. The mechanical rigidity of the extracellular matrix regulates the structure, motility, and proliferation of glioma cells. Cancer Res. 69, 4167–4174.

Unterhauser, F., Bosch, U., Zeichen, J., Weiler, A., 2004. α-Smooth muscle actin containing contractile fibroblastic cells in human knee arthrofibrosis tissue. Arch. Orthop. Trauma Surg. 124, 585–591.

Vincent, L.G., Choi, Y.S., Alonso-Latorre, B., del Álamo, J.C., Engler, A.J., 2013. Mesenchymal stem cell durotaxis depends on substrate stiffness gradient strength. Biotechnol. J. 8, 472–484.

Walcott, S., Sun, S.X., 2010. A mechanical model of actin stress fiber formation and substrate elasticity sensing in adherent cells. Proc. Natl. Acad. Sci. 107, 7757–7762.

Wang, A.Z., Chen, J.M., Fisher, G.W., Wang, J.C., Diamond, H.S., 1994. Improved in vitro models for assay of rheumatoid synoviocyte chemotaxis. Clin. Exp. Rheumatol. 12, 293–299.

Wang, J., Lin, J.-S., 2007. Cell traction force and measurement methods. Biomech. Model Mechanobiol. 6, 361–371.

Wang, P.-Y., Tsai, W.-B., Voelcker, N.H., 2012. Screening of rat mesenchymal stem cell behaviour on polydimethylsiloxane stiffness gradients. Acta Biomater. 8, 519–530.

Winer, J.P., Oake, S., Janmey, P.A., 2009. Non-linear elasticity of extracellular matrices enables contractile cells to communicate local position and orientation. PLoS ONE 4, e6382.

Yeung, T., Georges, P.C., Flanagan, L.A., Marg, B., Ortiz, M., Funaki, M., Zahir, N., Ming, W., Weaver, V., Janmey, P.A., 2005. Effects of substrate stiffness on cell morphology, cytoskeletal structure, and adhesion. Cell Motil. Cytoskelet. 60, 24–34.

Zemel, A., Rehfeldt, F., Brown, A.E.X., Discher, D.E., Safran, S.A., 2010. Cell shape, spreading symmetry, and the polarization of stress-fibers in cells. J. Phys.: Condens. Matter 22, 194110.